Thermalization of long range Ising model in different dynamical regimes: a full counting statistics approach.

Nishan Ranabhat[1,2⋆], Mario Collura[1]

1 SISSA - International School for Advanced Studies, via Bonomea 265, 34136 Trieste, Italy
2 The Abdus Salam International Centre for Theoretical Physics, Strada Costiera 11, 34151 Trieste, Italy
⋆ nranabha@sissa.it

December 2, 2022

arXiv:2212.00533v1 [cond-mat.stat-mech] 1 Dec 2022

Abstract

We study thermalization of transverse field Ising chain with power law decaying interaction $\sim 1/r^{\alpha}$ following a global quantum quench of the transverse field to two different dynamical regimes. We quantify the thermalization behavior by comparing the full probability distribution function (PDF) of the evolving states with the corresponding thermal state given by the Gibbs canonical ensemble (GCE). To this end, we use matrix product state (MPS) based time dependent variational principle (TDVP) algorithm to simulate both real time evolution following a global quantum quench and the finite temperature density operator. We observe that thermalization is strongly suppressed in the region with strong confinement for all the interaction strength α considered whereas thermalization occurs in the region with weak confinement.

Contents

1 Introduction 2

2 Model and Methods 3

3 Numerical details 5
3.1 Quench protocol and pure state evolution 5
3.2 Simulation of finite temperature states 5
3.3 Extracting effective temperature 6

4 Results 7

5 Conclusion 9

A Simulation of finite temperature density operator with tensor networks 9

B Thermal phase transition in long range Ising model 11

C Confinement dynamics in different regimes 11

References 18

1 Introduction

The dynamics of isolated manybody system out of equilibrium has been studied profusely in recent decades and is driven by corresponding advances in the engineering of the synthetic quantum matter in laboratory [1–11] and both analytical and numerical techniques [12–25]. An age old problem in quantum manybody dynamics is to study if a closed system kicked out of equilibrium eventually thermalizes i.e. the long time behavior of the dynamical system can be predicted by statistical mechanics. A generic non-integrable closed system is expected to thermalize according to the Eigenstate thermalization hypothesis (ETH) [26–30]. There are however studies that suggest otherwise [31–34], at least in the regime and time scale of their study. For a closed system initialized in a generic state, $|\psi_i\rangle$ (not the eigenstate of the Hamiltonian) and evolved with a unitary dynamics with a non-integrable Hamiltonian, H, thermalization is said to occur if the local observables eventually relaxes to an equilibrium value and matches the one predicted by the thermal ensemble,

$$\langle\hat{O}\rangle_{\text{eq}} = \langle\hat{O}\rangle_{\text{MCE}} = \frac{1}{N_{E_i,\delta\mathcal{E}}} \sum_{|E_n - E_i| < \delta\mathcal{E}} \langle\psi_n|\hat{O}|\psi_n\rangle\,, \tag{1}$$

$$\langle\hat{O}\rangle_{\text{eq}} = \langle\hat{O}\rangle_{\text{CGE}} = \frac{\text{Tr}(\rho_\beta \hat{O})}{\text{Tr}(\rho_\beta)}. \tag{2}$$

Equation 1 suggests thermalization according to microcanonocal ensemble (MCE), the sum is taken over all eigenstates of Hamiltonian in the narrow energy range $\delta\mathcal{E}$ around the initial energy $E_i = \langle\psi_i|H|\psi_i\rangle$, $N_{E_i,\delta\mathcal{E}}$ is the normalization factor counting the energy eigenstates in the range $2\delta\mathcal{E}$. This approach requires the full diagonalization [28,35,36] or partial diagonalization around the initial energy density [37] of the Hamiltonian and is therefore computationally constrained by the total system size that can be studied. Equation 2 suggests thermalization according to canonical Gibbs ensemble (CGE) and the trace is take over the density operator ρ_β defined at the inverse temperature $\beta = 1/T$ and fixed by the initial energy of the system, $E_i = \frac{\text{Tr}(\rho_\beta H)}{\text{Tr}(\rho_\beta)}$. Details on how to extract β and ρ_β follows in section 3 and appendix A. The conditions 1 and 2 are what is known as the strong thermalization. A weak thermalization condition follows where not the equilibrium value but the time average of the local order parameter converges to the thermal prediction [33,34].

Disordered systems exhibiting manybody localization is shown to suppress thermalization [38–41]. In clean systems dynamical confinement suppresses information spreading and thermalization mechanism [42–45]. Long range Ising model (LRIM) exhibits confinement [44,45], see appendix C, and a recent study [4] observes suppression of thermalization in the confined regime of LRIM simulated with trapped ions. Furthermore, using high scale exact diagonalization the validity of ETH has been tested for different range of interaction strength, α (see 2), of LRIM and it is shown that strong ETH typically holds at least in the range $\alpha \geq 0.6$ [35]. Previously, we studied the relaxation of order parameter statistics after a global quench [46] which showed two

distinct dynamical regimes based on the gaussification of the full counting statistics (FCS) of the subsystem magnetization. Building on that work, here we will investigate the thermalization of LRIM according to CGE following a global quench to different dynamical regimes. We will test the thermalization with the most stringent condition by comparing the FCS of the time evolving state after a global quench with the FCS of the corresponding thermal state.

This article is structured as follows: In section 2 we introduce the model, order parameter and its distribution, and a metric to measure the proximity of the time evolved state to the thermal state. In section 3 we detail the numerical methods, specifically the evolution of pure state, simulation of thermal state, and the extraction of the effective temperature attributed to a global quench. This section is complimented by appendix A. In section 4 we present the results of our study. Additional informations are collected in appendices B and C. Finally, we summarize and present possible future research direction in section 5.

2 Model and Methods

We study the ferromagnetic long range Ising model (LRIM) with the Hamiltonian,

$$H(\alpha, h/J) = -\frac{1}{\mathcal{K}(\alpha)} \sum_{i<j}^{N} \frac{|J|}{|i-j|^{\alpha}} \hat{s}_i^x \hat{s}_j^x - h \sum_{i=1}^{N} \hat{s}_i^z \tag{3}$$

where $\hat{s}_i^{\mu}, \mu = x, y, z$ is the spin one-half matrices at site i. We assume open boundary condition which is relevant to experimental setup and numerical methods. The ferromagnetic spin to spin interaction is given by the inverse of the distance between the spins raised to the power $\alpha \geq 0$. For $\alpha \leq 1$ the inverse power law interaction series is divergent with the lattice size and is normalized with Kac normalization constant

$$\mathcal{K}(\alpha) = \frac{1}{N-1} \sum_{i<j}^{N} \frac{1}{|i-j|^{\alpha}} = \frac{1}{N-1} \sum_{n=1}^{N} \frac{N-n}{n^{\alpha}}. \tag{4}$$

The Kac normalization ensures the intensivity of the energy density in the $\alpha \leq 1$ regime. The static and dynamical behavior of this model is strictly governed by the interaction strength α. At $\alpha = \infty$ the model reduces to the transverse field Ising model (TFIM) which is exactly solvable by mapping to a system of spinless fermions via Jordan-Wigner transformations [47]. TFIM shows a quantum phase transition from ferromagnetic to paramagnetic phase at $h = J/2$; the quantum phase transition persists with decreasing α albeit with increasing h [5, 48–50]. The other extreme at $\alpha = 0$ is the fully connected regime and is analytically tractable for both static and dynamical properties [46, 51, 52]. The model exhibits long range ferromagnetic order at low finite temperature for $\alpha < 2$ [53, 54]. As there is no spontaneous symmetry breaking in finite systems and the model 3 is $\mathbb{Z}_2$ symmetric, the finite temperature states with ferromagnetic order also have $\mathbb{Z}_2$ symmetry, see appendix B. The region $\alpha < 2$ is extremely rich, and exhibits a plethora of exotic phenomenons like prethermalization [11], nonlinear propagation of light cones [55, 56], dynamical phase transition [2, 3, 46, 57–59], dynamical confinement [4, 44, 45]. Furthermore, the increased interest in this model is also due to its great experimental relevance, primarily with systems of trapped ions with controllable strength of the transverse field and interaction range. Several static and dynamical properties of LRIM have been studied in lab so far [1–4, 11].

The full information of a generic time evolving quantum state of a spin system expanded in the computational basis, $|\psi_t\rangle = \sum_{\{\sigma_i\}} C_{\{\sigma_i\}}(t)\,|\sigma_i, \sigma_2, ..., \sigma_i, ..., \sigma_N\rangle$, is included in the set of coefficient $\{C_{\{\sigma_i\}}(t)\}$. The number of coefficients scales exponentially with the number of spins making many body systems extremely difficult to study. A general approach to study dynamics in many body system is to track the evolution of the expectation value of a local observable $\langle\psi_t|\hat{O}|\psi_t\rangle$, like for example the order parameter in a system which may exhibit an order-disorder transition. A more robust approach instead is to track the full probability distribution function (PDF) of such observable as it includes the detailed information (all the moments and cumulants of the distribution) about the quantum fluctuation of the system. Notably, if $\hat{O}$ is diagonal in the computational basis then the corresponding PDF is defined as

$$P(O,t) = \sum_{\{\sigma_i\}} \left|C_{\{\sigma_i\}}(t)\right|^2 \quad \forall\{\sigma_i\} : \langle\sigma_1, \sigma_2, ..., \sigma_i, ..., \sigma_N|\hat{O}|\sigma_1, \sigma_2, ..., \sigma_i, ..., \sigma_N\rangle = O \tag{5}$$

which is just the histogram of the square of coefficients of the many-body wave function in the range of the possible outcomes of the measurements of $\hat{O}$. From the PDF, moments(or cumulants) of any order can be easily calculated. For the entirety of this work we fix the eigenvectors of the total spin operator in longitudinal direction, i.e. $\hat{S}^x = \sum_{i=1}^{N} \hat{s}_i^x$ as our computational basis. For our setup the order parameter of interest is the longitudinal magnetization defined on a subsystem l in the system of N spins

$$\hat{M}_l = \sum_{i=1}^{l} \hat{s}_i^x. \tag{6}$$

$\hat{M}_l$ is a suitable observable as it generically relaxes to a stationary state [60], eventually approaching a stationary statistical distribution in a subsystem of dimension l. Furthermore, $\hat{M}_l$ is diagonal in the computational basis so the definition 5 applies. The probability distribution function of the subsystem magnetization $\hat{M}_l$ defined in a generic state ρ_t (pure or mixed) is given by

$$P_l(m,t) = \mathrm{Tr}(\rho_t\,\delta(\hat{M}_l - m)) \tag{7}$$

which can be Fourier transformed to an integral

$$P_l(m,t) = \int_{-\pi}^{\pi} \frac{d\theta}{2\pi} e^{-i\theta m} \mathrm{Tr}\left(\rho_t e^{i\theta\hat{M}_l}\right) \tag{8}$$

where $G_l(\theta,t) = \mathrm{Tr}\left(\rho_t e^{i\theta\hat{M}_l}\right)$ is the moment generating function. Since the Hamiltonian 3 is a system of spin one-half, m can take integer(half-integer) values in the range $m \in \left\{-\frac{l}{2}, -\frac{l}{2}+1, ..., \frac{l}{2}-1, \frac{l}{2}\right\}$ if l is even(odd). Historically, PDF was studied as full counting statistics (FCS) of the electron fluctuation in mesoscopic systems [61–63]. Recently, FCS is studied in quantum many body systems in both equilibrium and nonequilibrium regimes [18, 19, 43, 46, 64–69].

To quantify thermalization we introduce a metric Distance to thermalization, $DT(t)$ which was first introduced in [70]. It is the Euclidean distance between the PDF of the order parameter at time t after the quantum quench, $P_l(m,t)$ and the corresponding thermal PDF, $P_l^{\mathrm{TH}}(m)$ i.e.

$$DT(t) = \sqrt{\sum_m \left[P_l(m,t) - P_l^{\mathrm{TH}}(m)\right]}. \tag{9}$$

The convergence of the PDF is a more stringent condition for thermalization than the convergence of the expectation value as the former implies the later but the later doesn't necessarily implies the former. Similar approach has been used to investigate thermalization in some studies [37,69–71]. The details on how to extract the thermal state corresponding to a global quantum quench is discussed in detail in 3.3. If the system thermalizes $DT(t)$ should converge to zero in the long time limit.

3 Numerical details

The numerical simulations in this work falls on two categories;

- real time evolution of pure state following a global quench.
- simulation of finite temperature density operators.

We use matrix product state (MPS) based Time Dependent Variational Principle (TDVP) algorithm [23,24] for both real time evolution of pure state and simulating finite temperature density operators. This approach gives us an advantage over exact diagonalization methods as we can simulate system of sizes much larger than the current capability of exact diagonalization techniques.

3.1 Quench protocol and pure state evolution

The quench protocol is as follows (energy is rescaled to $|J| = 1$ from here on): At time $t = 0$ we prepare the system as the ground state of the Hamiltonian, $H_i(\alpha, 0)$ which is a $\mathbb{Z}_2$ symmetric GHZ [72,73] state along longitudinal direction

$$|\psi_i\rangle = \frac{1}{\sqrt{2}}(|\rightarrow, \ldots \rightarrow, \rightarrow, \rightarrow \ldots, \rightarrow\rangle + |\leftarrow, \ldots \leftarrow, \leftarrow, \leftarrow \ldots, \leftarrow\rangle), \tag{10}$$

such that,

$$\hat{s}^x |\rightarrow\rangle = |\rightarrow\rangle \quad \text{and} \quad \hat{s}^x |\leftarrow\rangle = -|\leftarrow\rangle . \tag{11}$$

Equation 10 can be written as an exact MPS with bond dimension $\chi = 2$. We perform a global quench along the transverse field h to a final Hamiltonian $H_f(\alpha, h)$ while keeping the interaction strength α constant. Subsequently, we evolve the system unitarily as $|\psi_{t+dt}\rangle = e^{-idtH_f} |\psi_t\rangle$ and keep track the evolution by calculating the FCS of the order parameter at each time step. The unitary time evolution is performed using TDVP with second order integration scheme. For our simulation we have fixed the maximum bond dimension $\chi_{max} = 128$ and a trotter time-step of $dt = 0.05$. There is a finite time step error of $O(dt^3)$ per time step and $O(dt^2)$ per unit time [74].

3.2 Simulation of finite temperature states

The finite temperature states can be simulated by casting the density operator as locally purified tensor network [75,76]. The finite temperature states are described by the density operator given by Gibbs distribution $\rho(\beta) = \frac{e^{-\beta H}}{Tr[e^{-\beta H}]}$ where $\beta = \frac{1}{T}$ is the inverse temperature. At $\beta = 0$ (infinite temperature) the state is maximally mixed and is given as the tensor product of local identities

$\rho_0 = \bigotimes_{i=1}^{N} \mathbf{1}^{\sigma_i,\tilde{\sigma}_i} = \mathbb{1}$, where each $\mathbf{1}^{\sigma_i,\tilde{\sigma}_i}$ is a unit matrix of size (d,d), i.e. $\mathbf{1}^{\sigma_i,\tilde{\sigma}_i} = [\delta_{\sigma_i,\tilde{\sigma}_i}]_{d\times d}$ and d is the dimension of the physical space (for spin $\frac{1}{2}$, $d=2$). The density operator for any finite temperature (non-zero β) is

$$\rho_\beta \propto e^{-\beta H} = e^{-\frac{\beta}{2}H}\mathbb{1}e^{-\frac{\beta}{2}H} \tag{12a}$$

$$\propto e^{-\frac{\beta}{2}H}\rho_0 e^{-\frac{\beta}{2}H} \tag{12b}$$

We keep the density operator operator in locally purified form $\rho = \mathbf{X}\mathbf{X}^\dagger$ at each stage where $\mathbf{X}$ is represented as tensor

$$\mathbf{X}^{\sigma_1,\sigma_2,\ldots\sigma_i,\ldots,\sigma_N}_{k_1,k_2,\ldots,k_i,\ldots,k_N} = A^{\sigma_1,k_1}_{m_0,m_1} A^{\sigma_2,k_2}_{m_1,m_2}\ldots A^{\sigma_i,k_i}_{m_{i-1},m_i}\ldots A^{\sigma_N,k_N}_{m_{N-1},m_N} \tag{13}$$

where $s_i = d$, $k_i = d$ are the physical index and the Kraus index are are fixed through out and $1 \le m_i \le \chi_{max}$ is the bond index and χ_{max} is the maximum value of bond dimension. The density operator initialized at infinite temperature can now be purified to a finite temperature in trotterized steps

$$\rho_{\beta+d\beta} = e^{-\frac{d\beta}{2}H}\rho_\beta e^{-\frac{d\beta}{2}H} \tag{14a}$$

$$= e^{-\frac{d\beta}{2}H}\mathbf{X}\mathbf{X}^\dagger e^{-\frac{d\beta}{2}H} \tag{14b}$$

$$= e^{-\frac{d\beta}{2}H}\mathbf{X}[e^{-\frac{d\beta}{2}H}\mathbf{X}]^\dagger \tag{14c}$$

Equation 14 can be simulated using imaginary time TDVP ($-idt \to -d\beta$) in only the half section of the density operator operator and never contracting the X and $X^\dagger$ layer during the evolution, thus strictly preserving the locally purified form. The diagrammatic details on how to simulate finite temperature density operators using imaginary time TDVP and calculate the observables is explained in Appendix A. For our simulation of finite temperature density operator we have fixed $\chi_{max} = 128$ and the trotterized time-step $d\beta = 0.001$. The smaller trotter time step is essential for reducing the error in the extraction of effective temperature.

3.3 Extracting effective temperature

A global quench $H_i(\alpha,0) \longrightarrow H_f(\alpha,h)$ in an isolated system adds an extensive amount of energy to the system and as a consequence the system relaxes to a state which is higher in energy scale than the ground state of the post quench Hamiltonian [60] i.e.

$$\lim_{N\to\infty}\frac{1}{N}\frac{\langle\psi_t|H_f|\psi_t\rangle}{\langle\psi_t|\psi_t\rangle} > \lim_{N\to\infty}\frac{1}{N}\frac{\langle\psi_0|H_f|\psi_0\rangle}{\langle\psi_0|\psi_0\rangle} \tag{15}$$

where $|\psi_0\rangle$ is the ground state of the post quench Hamiltonian $H_f(\alpha,h)$. The left hand side of equation 15 is a constant in time since the real time evolution of $|\psi_t\rangle$ is unitary. The temperature attributed to a quench is called the effective temperature, β_{eff} which is the temperature at which the thermal energy density above the ground state of the post quench Hamiltonian matches the energy density of the post quench system,

$$\frac{1}{N}\frac{\langle\psi_t|H_f|\psi_t\rangle}{\langle\psi_t|\psi_t\rangle} = \frac{1}{N}\frac{Tr(\rho_\beta H_f)}{Tr(\rho_\beta)}. \tag{16}$$

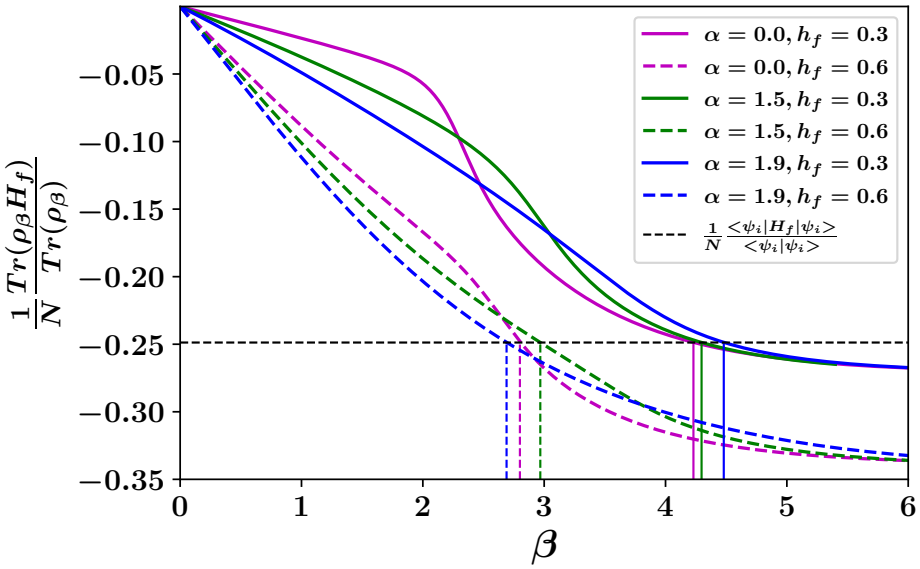


Figure 1: Numerical extraction of β_{eff} corresponding to a global quantum quench. The horizontal black dashed line represent the energy density attributed to the quench. The colored lines represents the energy density as the function of inverse temperature β for the corresponding post quench parameter (in legend). The point at which the colored lines intersects the black dashed lines represents β_{eff} for the corresponding post quench parameters (represented by vertical colored lines). See 3.3 for details.

The effective temperature β_{eff} is extracted by solving the equation 16. The left hand side of the equation is trivially calculated as $\langle\psi_t|H_f|\psi_t\rangle = \langle\psi_i|e^{itH_f}H_f e^{-itH_f}|\psi_i\rangle = \langle\psi_i|H_f|\psi_i\rangle$, the right hand side can be calculated for a series of β by numerically solving the equation 14 and calculating the energy density at each instances. As mentioned in 3.2 the precision in the extraction of β_{eff} depends on the trotter steps $d\beta$ in the solution of equation 14. In Fig. 1 we plot the numerical solution of equation 16. The energy density attributed to quench (represented by black dashed line) in our setup is independent of the post quench parameters because the spin-spin interaction term in Hamiltonian 3 is normalized with the Kac normalization 4 whereas the expectation value $h\langle\psi_i|\sum_j \hat{s}_j^z|\psi_i\rangle$, taken over the transverse field term is trivially zero. If we extend the simulation to larger β (i.e. lower temperature) all the curves will converge to the ground state energy density of H_f at the corresponding post quench parameters. Once β_{eff} is extracted we can calculate the corresponding thermal PDF, $P^{\mathrm{TH}}(m) = P^{\beta_{eff}}(m)$ following equation 8.

4 Results

Our main focus is to study the convergence of the metric $DT(t)$ at two different dynamical phases of the LRIM as the convergence of $DT(t)$ to zero suggests thermalization in that particular phase. For all the quenches we prepare our initial state as the $\mathbb{Z}_2$ symmetric GHZ state 10 which is the ground state of the Hamiltonian 3. We choose this initial state instead of the more common (and easily prepared in laboratory [4]) fully polarized state because the model 3 thermally transits from paramagnetic phase, with Gaussian PDF, at high temperature to a ferromagnetic phase with

a $\mathbb{Z}_2$ symmetric bimodal PDF, see appendix B. We keep $\alpha < 2$ as it is a more interesting region that exhibits both finite temperature phase transition [77, 78] and dynamical phase transitions [2, 3, 46, 57–59]. We take three different values of interaction strength, $\alpha \in \{0.0, 1.5, 1.9\}$. At $\alpha = 0.0$ the system is integrable as it is fully connected and has full permutation symmetry so we don't expect thermalization. The other two values are chosen as $\alpha = 1.5$ and $\alpha = 1.9$ because the system exhibits relatively faster equilibration (and Gaussification of PDF) for these values following a quench to the dynamical paramagnetic phase [46].

In Figs. 2 we plot the evolution of $DT(t)$ following a global quench of transverse field to $h_f = 0.3$ which is a dynamical ferromagnetic phase [46, 57] for all the values of α considered. In Fig. 2 (a) we observe that the $DT(t)$ shows oscillations well above the $DT = 0$ line. This is expected as $\alpha = 0$ is integrable and we don't expect thermalization. The behavior is robust for different system sizes, $l = \{20, 60, 100\}$. In Fig. 2 (d) we plot the PDFs for three different time slices during the evolution (scatter colored plots) and the PDF attributed to the corresponding thermal state (dashed black). We observe a similar oscillating behavior for $DT(t)$ in Figs. 2 (b),(c) with different characteristic frequencies. This is an unexpected behavior as the model is non-integrable in this regime and we expect thermalization to occur [26]. The explanation for the apparent suppression of thermalization lies in confinement behavior. In LRIM the long range interaction confines the lowly excited quasiparticles from spreading following a global quench thus suppressing the correlation spreading in the system [44,45], this in turn suppresses thermalization. We still expect thermalization to occur but only at a very large time scales [79]. In Figs. 11 (a) we plot the half-chain correlation spreading in time following a global quench to $\alpha = 1.9$ and $h_f = 0.3$, we see a strong signature of confinement with connected correlation function $\langle \sigma^x_{k+\Delta} \sigma^x_k \rangle_c$ oscillating in time, the frequency of which matches the frequency of oscillation of $DT(t)$ in Fig. 2 (c). In Figs. 2 (e),(f) the colored scattered plots shows the PDFs at three time slices following a global quench and the black dashed plots are the PDFs for corresponding thermal state. One important observation is that the thermal PDFs (black dashed) in Figs. 2 (e),(f) are bimodal suggesting long range ferromagnetic order, so if the system thermalizes for these post quench parameters in a long time limit it would exhibit long range ferromagnetic order. This further bolsters the claim that this is a dynamical ferromagnetic phase.

Figs. 3 is similar to Figs. 2 except that we now quench the system to $h_f = 0.6$ which corresponds to the dynamical paramagnetic phase [46, 57] for all the values of α considered. In Fig. 3 (a) we now observe equilibration of $DT(t)$, however the equilibrium value is way above $DT = 0$ (dashed black line). This is an expected behavior as $\alpha = 0$ is an integrable point. In Fig. 3 (b) we observe a different behavior, $DT(t)$ now converges to the vicinity of $DT = 0$, however in the time scale and the system size considered we don't observe a stable equilibration. Therefore, although $DT(t)$ is fairly close to $DT = 0$, there is a marked separation for all length scales considered. In Fig. 3 (c) however we observe that $DT(t)$ converges to $DT = 0$ and remains stable for the two higher subsystem sizes, $l = 60, 100$. This observation confirms that the system thermalizes for the corresponding global quench. A clearer picture is presented in Fig. 3 (f) where we see the late time PDF following the global quench (orange scatter plot) perfectly overlaps with the corresponding thermal PDF (black dashed plot). A very important observation is that although we observe thermalization in Fig. 3 (f) the system is still in the confined phase as seen in Fig. 11 (b) where we observe that the speed at which correlation is spreading is still slower than that of the short range case (see Fig. 11 (d)). In fact confinement persists to even higher values transverse field as seen in Fig. 11 (c), however the effect of confinement is heavily diluted for higher transverse field. Recent study observed confinement to deconfinement transition for a system of up to

31 spins for much higher transverse field [4]. This shows that only strong confinement suppresses thermalization whereas we can observe thermalization in presence of weak confinement.

5 Conclusion

We studied the relaxation dynamics of the long range Ising model following a global quantum quench of the transverse field and checked if the system thermalizes according to CGE in the time scale that is computationally viable. While the model is non-integrable for all values of α, except for the two extremes i.e. $\alpha = \{0.0, \infty\}$, and we expect thermalization to occur following a global quench, however at the same time LRIM shows confinement which suppresses information spreading and eventually thermalization. Starting from the GHZ state we quenched the system to two different dynamical regimes. As expected strong confinement impedes thermalization for smaller quenches, i.e. to the dynamical ferromagnetic region, where the metric DT showed persistent oscillations characteristics to the masses of bound mesons. For quenches to the dynamical paramagnetic region we observe a characteristically different behavior. The persistent oscillation is absent and DT relaxes much faster. While we don't observe a conclusive evidence of thermalization for $\alpha = 1.5$, we see a strong signature of thermalization in DT for $\alpha = 1.9$. So while strong confinement suppresses thermalization we observe thermalization in the weak confinement regime. This observation opens up new avenues for the study of thermalization of systems in strong and weak confinement regimes.

Recently the relaxation dynamics of transverse Ising model with longitudinal field was studied [79]. This is another paradigmatic model that exhibits confinement. In that work, the authors show that thermalization following a global quench occurs in multiple stages with a well defined timescales. They observe that the system first relaxes towards a prethermal state with fixed number of mesons. Only in exponentially long time limit the meson number conservation is violated leading to true thermalization.

Therefore, a natural direction for future research is to conduct a similar study in the LRIM by defining time scales of relaxation for quenches in different dynamical regimes and the underlying mechanism governing them. An open question indeed is whether the thermalization we observed is a true thermalization following the violation of meson number conservation, or just a prethermal state which is very close to the thermal one.

Acknowledgements

Nishan Ranabhat thanks Alvise Bastianello for fruitful discussion and suggesting the future extension of the work. The numerical simulation of this project was performed at the Ulysses v2 cluster at SISSA.

A Simulation of finite temperature density operator with tensor networks

We start at infinite temperature i.e. $\beta = 0$ where density operator $\rho_{\beta=0}$ is maximally mixed and is proportional to the identity matrix of size $(2^d, 2^d)$. Physically, this represents the uniform mixture

of all the basis states. The big identity can be written as a tensor product of local identities as shown in Fig. 4.

Rather than working with the density operator as an MPO we represent the density operator in the locally purified form [80, 81] which is positive semi-definite by construction and keep it in locally purified form at every stage of the thermal purification process. In Fig. 5 we represent $\rho_{\beta=0}$ in the locally purified form $\mathbf{X}_{\beta=0}\mathbf{X}^{\dagger}_{\beta=0}$.

With density operator in this form we can evolve one of the halves ($\mathbf{X}$ or $\mathbf{X}^{\dagger}$) as shown in equation 14 and the evolution on the other half is its trivial conjugate. This approach is computationally efficient as we can work with cheaper MPS instead of more expensive MPDO. In Fig. 6 one half of the $\rho_{\beta=0}$ in locally purified form is shown, form here on we will only work with this half.

Algebraically, $\mathbf{X}_{\beta=0}$ can be written as

$$\mathbf{X}^{\sigma_1,k_1,\ldots\sigma_i,k_i,\ldots,\sigma_N,k_N} = A^{\sigma_1,k_1} \otimes \ldots A^{\sigma_i,k_i} \ldots \otimes A^{\sigma_N,k_N} \tag{17}$$

where σ (in black) represents the physical index and k (in red) represents an auxiliary index called the Krauss index. For the system of spin one-half particles we choose A as

$$A^{\sigma_i,k_i} = \frac{1}{\sqrt{2}}\begin{pmatrix} 1 & 0 \\ 0 & 1 \end{pmatrix} \qquad \forall\ i \in \{1,2,\ldots,N\} \tag{18}$$

as shown in Fig. 7. This particular choice is taken to preserve the trace of the density operator as with this choice we have

$$\sum_k A^{\sigma,k}\tilde{A}^{\sigma,k} = \frac{1}{2}\begin{pmatrix} 1 & 0 \\ 0 & 1 \end{pmatrix} \tag{19}$$

such that the trace is 1, with this choice of $A^{\sigma,k}$ the entire density operator can be normalized to have a unit trace.

Finally, we reshape $\mathbf{X}_{\beta=0}$ from a string of 2×2 matrices to a string of four legged tensors of shape $(1,2,2,1)$ as shown in Fig. 8, which is a MPS of bond dimension 1.

Now that we have our initial state as an MPS, we can simulate a finite temperature density operator by following the equation 14. We only need to solve the first part of the equation i.e.

$$\mathbf{X}_{\beta+d\beta} = e^{-\frac{d\beta}{2}H}\mathbf{X}_{\beta}. \tag{20}$$

The other half is its trivial conjugate by construction. Numerically equation 20 can be solved for long range spin systems by imaginary time (i.e. $idt \to d\beta$) TDVP. The TDVP algorithm for the simulation of thermal state is exactly the same as the imaginary time TDVP for pure state evolution with three legged MPS. The only difference is that the MPS here has an extra leg representing the Krauss index, however, the Krauss index in thermal purification process is obsolete (in dissipative systems there is contraction also along the Krauss index [80]) and the Hamiltonian MPO and other physical operators act only in the physical index σ. In Fig. 9 we show the tensor network diagram for the calculation of the expectation value of a two legged operator $\hat{O}_i$ acting on site i over the thermal state ρ_β. We see that the Krauss indices are contracted with each other at all sites whereas the operator acts only on the physical index at site i.

B Thermal phase transition in long range Ising model

For $\alpha > 2$ the long range Ising model is in the short range regime and doesn't show any finite temperature phase transition [77]. The critical properties of the thermal phase transition in quantum long range Ising model for $\alpha \leq 2$ has been thoroughly studied using the numerically exact path integral monte carlo methods [78]. In Figs. 10 we qualitatively show the thermal phase transition for $\alpha = \{1.5, 1.9\}$ and $h = \{0.3, 0.9\}$ respectively. As explained in 3 we begin with a maximally mixed state at $\beta = 0$ which is signified by a sharp Gaussian distribution of $P(m)$ (colored in red) centered at $m = 0$. The system is in deep paramagnetic phase at this point. As we cool down the system in the direction of increasing β the distribution becomes broader and around the critical temperature becomes essentially flat (colored in magenta). Further decreasing the temperature we see a bimodal distribution of $P(m)$ signifying the ferromagnetic phase. It is interesting to note that the system transits from a unimodal Gaussian distribution to a bimodal distribution which signifies the fact that the long range Ising Hamiltonian is $\mathbb{Z}_2$ symmetric. This is the major reason that we initialized our state as a $\mathbb{Z}_2$ symmetric GHZ state and not fully polarized state, which is easier to prepare experimentally.

C Confinement dynamics in different regimes

Confinement in long range Ising model is due to the ferromagnetic long range interaction between the interacting spins, however the confinement dynamics is strong or weak or absent at different point in the phase space of the long range Ising model [44, 45]. In this section we provide detail numeric results for the correlation spreading in time of the long range Ising chain following a sudden quench to different post quench Hamiltonians starting from a fully polarized initial state $|\psi_i\rangle = |\leftarrow, \leftarrow, ..., \leftarrow, ..., \leftarrow, \leftarrow\rangle_x$. In Figs. 11 we study the spreading of connected correlation function $\langle \sigma^x_{k+\Delta} \sigma^x_k \rangle_c = \langle \sigma^x_{k+\Delta} \sigma^x_k \rangle - \langle \sigma^x_{k+\Delta} \rangle \langle \sigma^x_k \rangle$ in the chain with $N = 200$ spins and fixing $k = 100$ such that $1 \leq \Delta \leq 100$. In panels (a),(b),(c), we fix $\alpha = 1.9$ and vary there transverse field $h = 0.3, 0.6, 0.8$. We observe a strong signature of confinement in panel (a) which diminishes with increasing h in panels (b), and (c). This is expected as the transverse field competes against the long range interaction responsible for confinement. In panel (d) we observe a light cone spreading with $v_{max} = 2h$ which is the maximum velocity of correlation spreading in transverse field Ising model [42] which is expected as $\alpha = 3$ is a short range regime.

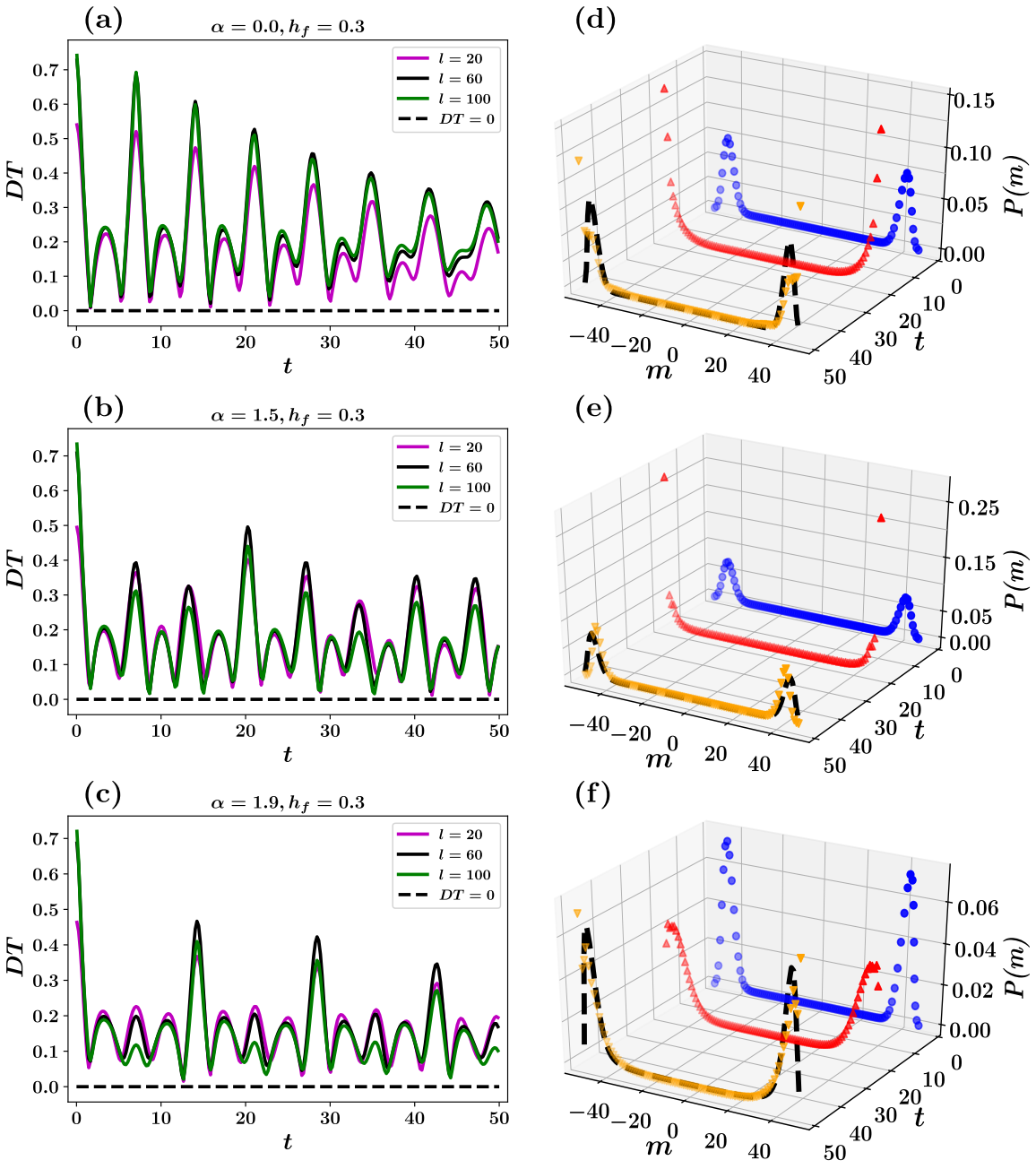


Figure 2: Time evolution of the metric DT following a global quantum quench to three values of interaction strength $\alpha \in \{0.0, 1.5, 1.9\}$ (first, second, and third row respectively) and transverse field $h_f = 0.3$ at three different subsystem sizes $l = \{20, 60, 100\}$ (represented by magenta, black, and green respectively). All three points are in dynamical ferromagnetic phases [46, 57]. The black dashed line in the plots in first column shows the $DT = 0$ line. In the second column we plot $P_l(m, t)$ with $l = 100$ at three time slices $t = \{2, 20, 50\}$ (represented by blue, red, and orange respectively). The black dashed curve represents the thermal PDF, $P^{\beta_{eff}}(m)$ attributed to the corresponding global quantum quenches.

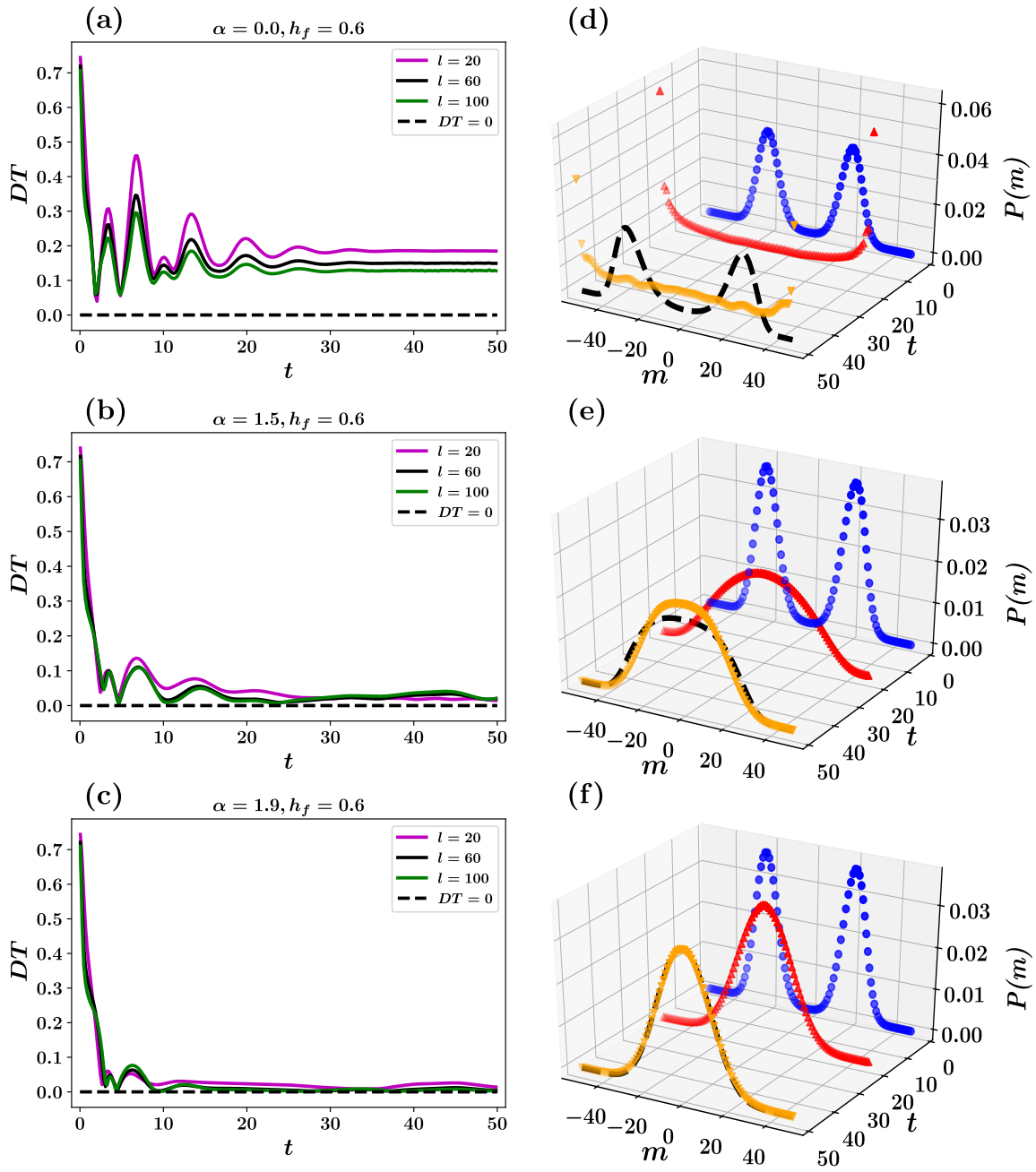


Figure 3: Time evolution of the metric DT following a global quantum quench to three values of interaction strength $\alpha \in \{0.0, 1.5, 1.9\}$ (first, second, and third row respectively) and transverse field $h_f = 0.6$ at three different subsystem sizes $l = \{20, 60, 100\}$ (represented by magenta, black, and green respectively). All three points are in dynamical paramagnetic phases [46, 57]. The black dashed line in the plots in first column shows the $DT = 0$ line. In the second column we plot $P_l(m, t)$ with $l = 100$ at three time slices $t = \{2, 20, 50\}$ (represented by blue, red, and orange respectively). The black dashed curve represents the thermal PDF, $P^{\beta_{eff}}(m)$ attributed to the corresponding global quantum quenches.

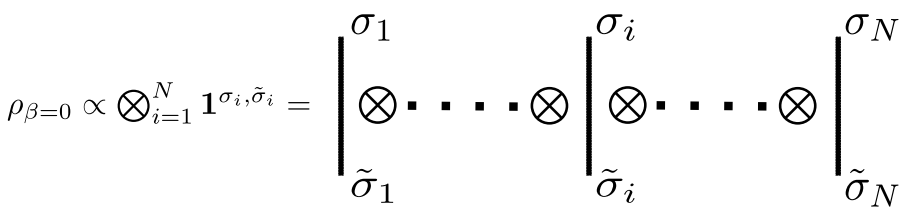


Figure 4: Maximally mixed density operator at $\beta = 0$ as the tensor product of local identities.

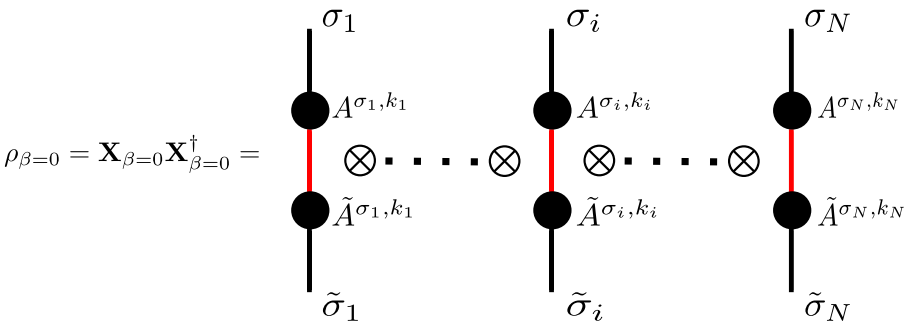


Figure 5: Representing $\rho_{\beta=0}$ in the locally purified form.

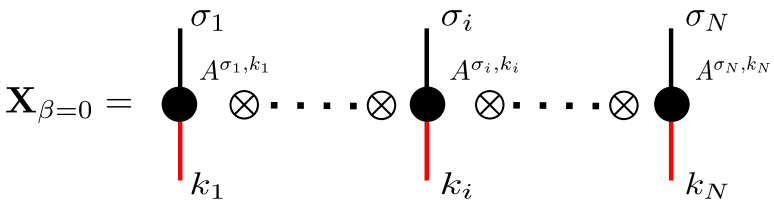


Figure 6: One half of the $\rho_{\beta=0}$ in the locally purified form.

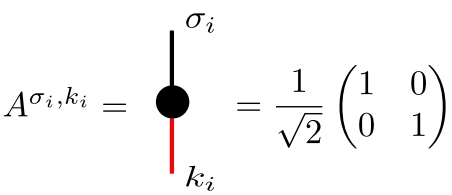


Figure 7: Choice of A^{σ_i,k_i} to preserve the trace of ρ.

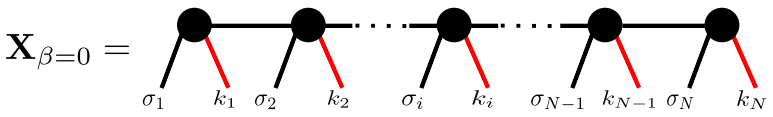


Figure 8: $\mathbf{X}_{\beta=0}$ in MPS form.

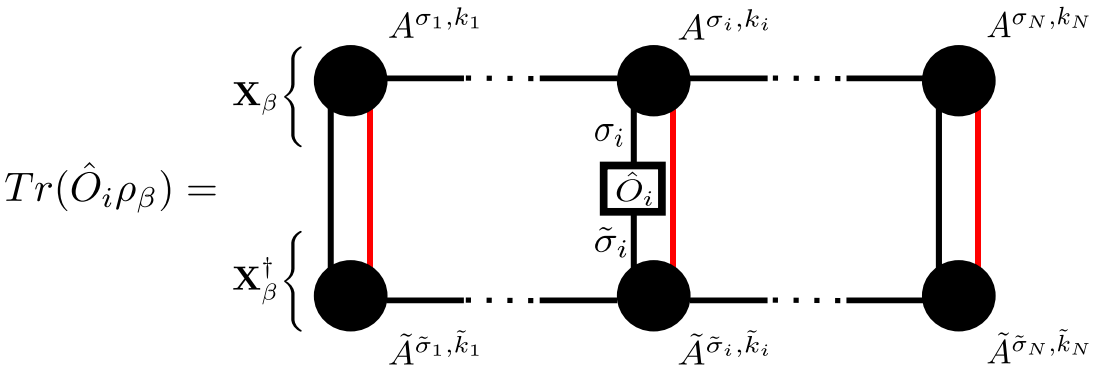


Figure 9: Expectation of local operator $\hat{O}_i$ in the thermal density operator ρ_β

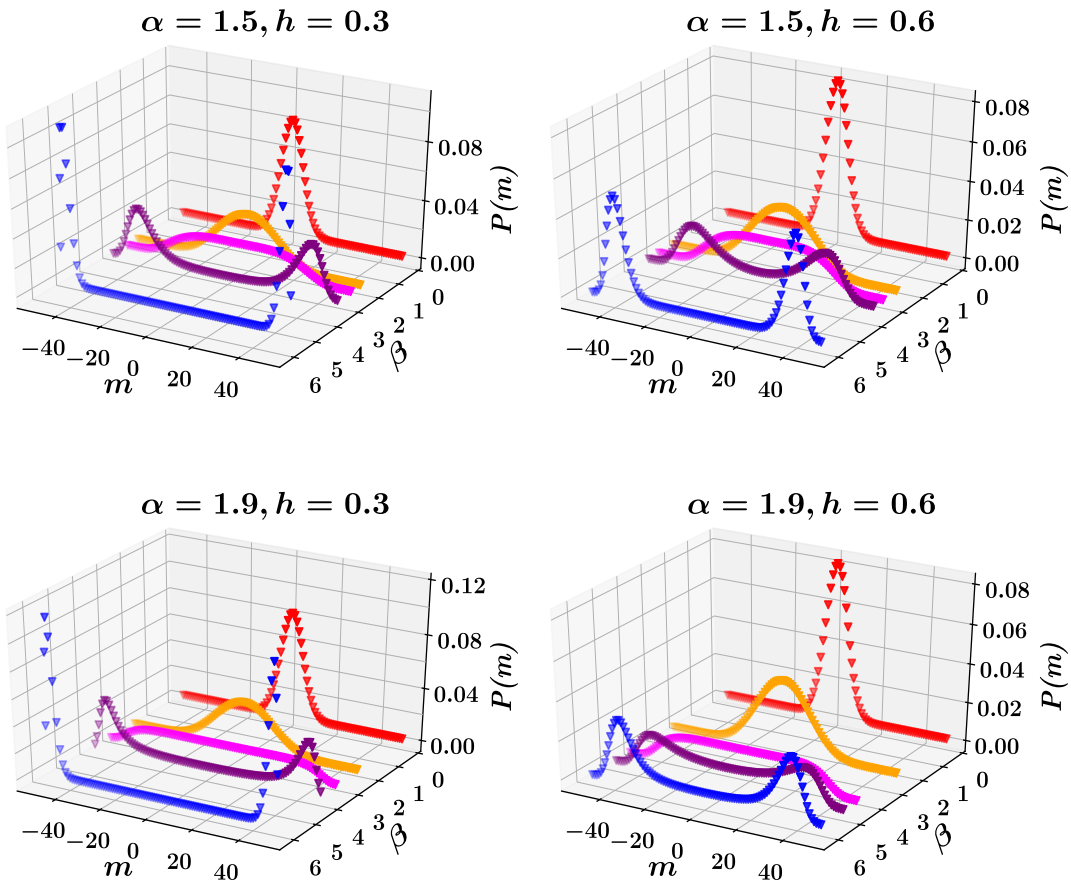


Figure 10: Thermal phase transition of long range Ising model at four different points in parameter space. The initial state in all cases is the maximally mixed state at infinite temperature represented by $\rho_{\beta=0}$, refer to 4. The color coding from red to blue signifies decreasing temperature .

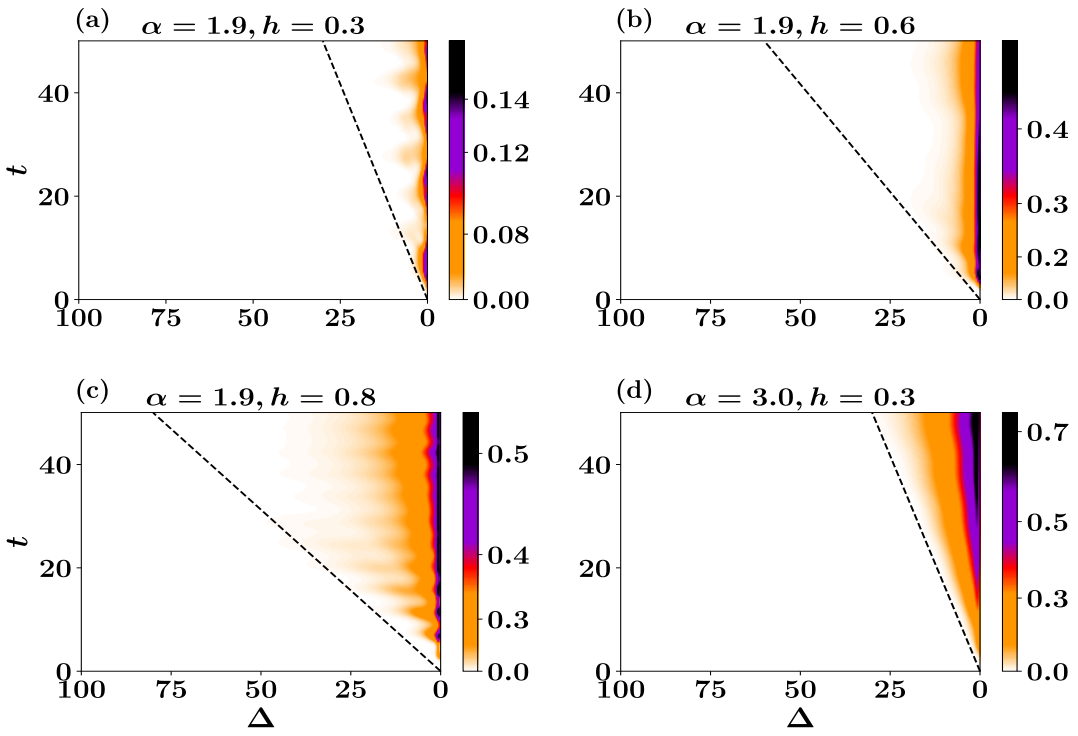


Figure 11: Real time dynamics of half chain connected correlation function $\left\langle \sigma_i^x \sigma_j^x \right\rangle_c$ after a global quantum quench of the transverse field starting from a fully polarized initial state. The dashed black lines is $v_{max} = 2h$ line for nearest neighbor transverse field Ising model [42].

References

[1] R. Islam, E. Edwards, K. Kim, S. Korenblit, C. Noh, H. Carmichael, G.-D. Lin, L.-M. Duan, C.-C. Joseph Wang, J. Freericks and C. Monroe, *Onset of a quantum phase transition with a trapped ion quantum simulator*, Nature Communications **2** (2011), doi:https://doi.org/10.1038/ncomms1374.

[2] J. Zhang, G. Pagano, P. W. Hess, A. Kyprianidis, P. Becker, H. Kaplan, A. V. Gorshkov, Z.-X. Gong and C. Monroe, *Observation of a many-body dynamical phase transition with a 53-qubit quantum simulator*, Nature **551**, 601 (2017), doi:https://doi.org/10.1038/nature24654.

[3] P. Jurcevic, H. Shen, P. Hauke, C. Maier, T. Brydges, C. Hempel, B. P. Lanyon, M. Heyl, R. Blatt and C. F. Roos, *Direct observation of dynamical quantum phase transitions in an interacting many-body system*, Phys. Rev. Lett. **119**, 080501 (2017), doi:10.1103/PhysRevLett.119.080501.

[4] W. L. Tan, P. Becker, F. Liu, G. Pagano, K. S. Collins, A. De, L. Feng, H. B. Kaplan, A. Kyprianidis, R. Lundgren, W. Morong, S. Whitsitt *et al.*, *Domain-wall confinement and dynamics in a quantum simulator*, Nature Physics **17**, 742747 (2021), doi:10.1038/s41567-021-01194-3.

[5] M. Knap, A. Kantian, T. Giamarchi, I. Bloch, M. D. Lukin and E. Demler, *Probing real-space and time-resolved correlation functions with many-body ramsey interferometry*, Phys. Rev. Lett. **111**, 147205 (2013), doi:10.1103/PhysRevLett.111.147205.

[6] J. Bohnet, B. Sawyer, J. Britton, M. Wall, A. Rey, M. Foss-Feig and J. Bollinger, *Quantum spin dynamics and entanglement generation with hundreds of trapped ions*, Science **352**, 1297 (2016), doi:10.1126/science.aad9958.

[7] T. Kinoshita, T. Wenger and D. Weiss, *A quantum newton's cradle*, Nature **440**, 900 (2006), doi:https://doi.org/10.1038/nature04693.

[8] T. Langen, R. Geiger and J. Schmiedmayer, *Ultracold atoms out of equilibrium*, Annual Review of Condensed Matter Physics **6**(1), 201 (2015), doi:10.1146/annurev-conmatphys-031214-014548.

[9] F. Meinert, M. J. Mark, E. Kirilov, K. Lauber, P. Weinmann, A. J. Daley and H.-C. Nägerl, *Quantum quench in an atomic one-dimensional ising chain*, Phys. Rev. Lett. **111**, 053003 (2013), doi:10.1103/PhysRevLett.111.053003.

[10] C. Gross and I. Bloch, *Quantum simulations with ultracold atoms in optical lattices*, Science **357**, 995 (2017), doi:10.1126/science.aal3837.

[11] B. Neyenhuis, J. Zhang, P. W. Hess, J. Smith, A. C. Lee, P. Richerme, Z.-X. Gong, A. V. Gorshkov and C. Monroe, *Observation of prethermalization in long-range interacting spin chains*, Science Advances **3** (2017), doi:10.1126/sciadv.1700672.

[12] P. Calabrese, F. H. L. Essler and M. Fagotti, *Quantum quench in the transverse field ising chain: I. time evolution of order parameter correlators*, Journal of Statistical Mechanics: Theory and Experiment **2012**(07), P07016 (2012), doi:10.1088/1742-5468/2012/07/P07016.

[13] P. Calabrese, F. H. L. Essler and M. Fagotti, *Quantum quench in the transverse-field ising chain*, Phys. Rev. Lett. **106**, 227203 (2011), doi:10.1103/PhysRevLett.106.227203.

[14] P. Calabrese and J. Cardy, *Quantum quenches in extended systems*, Journal of Statistical Mechanics: Theory and Experiment **2007**(06), P06008 (2007), doi:10.1088/1742-5468/2007/06/P06008.

[15] P. Calabrese and J. Cardy, *Evolution of entanglement entropy in one-dimensional systems*, Journal of Statistical Mechanics: Theory and Experiment **2005**(04), P04010 (2005), doi:10.1088/1742-5468/2005/04/P04010.

[16] P. Calabrese and J. Cardy, *Time dependence of correlation functions following a quantum quench*, Phys. Rev. Lett. **96**, 136801 (2006), doi:10.1103/PhysRevLett.96.136801.

[17] J.-S. Caux and F. H. L. Essler, *Time evolution of local observables after quenching to an integrable model*, Phys. Rev. Lett. **110**, 257203 (2013), doi:10.1103/PhysRevLett.110.257203.

[18] S. Groha, F. H. L. Essler and P. Calabrese, *Full counting statistics in the transverse field Ising chain*, SciPost Phys. **4**, 043 (2018), doi:10.21468/SciPostPhys.4.6.043.

[19] M. Collura, *Relaxation of the order-parameter statistics in the Ising quantum chain*, SciPost Phys. **7**, 072 (2019), doi:10.21468/SciPostPhys.7.6.072.

[20] A. J. Daley, C. Kollath, U. Schollwöck and G. Vidal, *Time-dependent density-matrix renormalization-group using adaptive effective hilbert spaces*, Journal of Statistical Mechanics: Theory and Experiment **2004**(04), P04005 (2004), doi:10.1088/1742-5468/2004/04/P04005.

[21] S. R. White and A. E. Feiguin, *Real-time evolution using the density matrix renormalization group*, Phys. Rev. Lett. **93**, 076401 (2004), doi:10.1103/PhysRevLett.93.076401.

[22] G. Vidal, *Efficient simulation of one-dimensional quantum many-body systems*, Phys. Rev. Lett. **93**, 040502 (2004), doi:10.1103/PhysRevLett.93.040502.

[23] J. Haegeman, J. I. Cirac, T. J. Osborne, I. Pižorn, H. Verschelde and F. Verstraete, *Time-dependent variational principle for quantum lattices*, Phys. Rev. Lett. **107**, 070601 (2011), doi:10.1103/PhysRevLett.107.070601.

[24] J. Haegeman, C. Lubich, I. Oseledets, B. Vandereycken and F. Verstraete, *Unifying time evolution and optimization with matrix product states*, Phys. Rev. B **94**, 165116 (2016), doi:10.1103/PhysRevB.94.165116.

[25] G. Lami, G. Carleo and M. Collura, *Matrix product states with backflow correlations*, Phys. Rev. B **106**, L081111 (2022), doi:10.1103/PhysRevB.106.L081111.

[26] M. Srednicki, *Chaos and quantum thermalization*, Phys. Rev. E **50**, 888 (1994), doi:10.1103/PhysRevE.50.888.

[27] J. M. Deutsch, *Quantum statistical mechanics in a closed system*, Phys. Rev. A **43**, 2046 (1991), doi:10.1103/PhysRevA.43.2046.

[28] H. Kim, T. N. Ikeda and D. A. Huse, *Testing whether all eigenstates obey the eigenstate thermalization hypothesis*, Phys. Rev. E **90**, 052105 (2014), doi:10.1103/PhysRevE.90.052105.

[29] R. Steinigeweg, J. Herbrych and P. Prelovšek, *Eigenstate thermalization within isolated spin-chain systems*, Phys. Rev. E **87**, 012118 (2013), doi:10.1103/PhysRevE.87.012118.

[30] M. Rigol, V. Dunjko and M. Olshanii, *Thermalization and its mechanism for generic isolated quantum systems*, Nature **452**, 854858 (2008), doi:10.1038/nature06838.

[31] C. Kollath, A. M. Läuchli and E. Altman, *Quench dynamics and nonequilibrium phase diagram of the bose-hubbard model*, Phys. Rev. Lett. **98**, 180601 (2007), doi:10.1103/PhysRevLett.98.180601.

[32] S. R. Manmana, S. Wessel, R. M. Noack and A. Muramatsu, *Strongly correlated fermions after a quantum quench*, Phys. Rev. Lett. **98**, 210405 (2007), doi:10.1103/PhysRevLett.98.210405.

[33] F. Chen, Z.-H. Sun, M. Gong, Q. Zhu, Y.-R. Zhang, Y. Wu, Y. Ye, C. Zha, S. Li, S. Guo, H. Qian, H.-L. Huang *et al.*, *Observation of strong and weak thermalization in a superconducting quantum processor*, Phys. Rev. Lett. **127**, 020602 (2021), doi:10.1103/PhysRevLett.127.020602.

[34] M. C. Bañuls, J. I. Cirac and M. B. Hastings, *Strong and weak thermalization of infinite nonintegrable quantum systems*, Phys. Rev. Lett. **106**, 050405 (2011), doi:10.1103/PhysRevLett.106.050405.

[35] S. Sugimoto, R. Hamazaki and M. Ueda, *Eigenstate thermalization in long-range interacting systems*, Phys. Rev. Lett. **129**, 030602 (2022), doi:10.1103/PhysRevLett.129.030602.

[36] A. Russomanno, M. Fava and M. Heyl, *Quantum chaos and ensemble inequivalence of quantum long-range ising chains*, Phys. Rev. B **104**, 094309 (2021), doi:10.1103/PhysRevB.104.094309.

[37] K. R. Fratus and M. Srednicki, *Eigenstate thermalization and spontaneous symmetry breaking in the one-dimensional transverse-field ising model with power-law interactions*, doi:10.48550/ARXIV.1611.03992 (2016).

[38] D. A. Abanin, E. Altman, I. Bloch and M. Serbyn, *Colloquium: Many-body localization, thermalization, and entanglement*, Rev. Mod. Phys. **91**, 021001 (2019), doi:10.1103/RevModPhys.91.021001.

[39] C. Gogolin, M. P. Müller and J. Eisert, *Absence of thermalization in nonintegrable systems*, Phys. Rev. Lett. **106**, 040401 (2011), doi:10.1103/PhysRevLett.106.040401.

[40] R. Nandkishore and D. A. Huse, *Many-body localization and thermalization in quantum statistical mechanics*, Annual Review of Condensed Matter Physics **6**(1), 15 (2015), doi:10.1146/annurev-conmatphys-031214-014726, https://doi.org/10.1146/annurev-conmatphys-031214-014726.

[41] M. Fava, R. Fazio and A. Russomanno, *Many-body dynamical localization in the kicked bose-hubbard chain*, Phys. Rev. B **101**, 064302 (2020), doi:10.1103/PhysRevB.101.064302.

[42] M. Kormos, M. Collura, G. Takács and P. Calabrese, *Real-time confinement following a quantum quench to a non-integrable model*, Nature Physics **13**, 249246 (2017), doi:10.1038/nphys3934.

[43] R. J. V. Tortora, P. Calabrese and M. Collura, *Relaxation of the order-parameter statistics and dynamical inement*, EPL (Europhysics Letters) **132**(5), 50001 (2020), doi:http://dx.doi.org/10.1209/0295-5075/132/50001.

[44] A. Lerose, B. Žunkovič, A. Silva and A. Gambassi, *Quasilocalized excitations induced by long-range interactions in translationally invariant quantum spin chains*, Phys. Rev. B **99**, 121112 (2019), doi:10.1103/PhysRevB.99.121112.

[45] F. Liu, R. Lundgren, P. Titum, G. Pagano, J. Zhang, C. Monroe and A. V. Gorshkov, *Confined quasiparticle dynamics in long-range interacting quantum spin chains*, Phys. Rev. Lett. **122**, 150601 (2019), doi:10.1103/PhysRevLett.122.150601.

[46] N. Ranabhat and M. Collura, *Dynamics of the order parameter statistics in the long range Ising model*, SciPost Phys. **12**, 126 (2022), doi:10.21468/SciPostPhys.12.4.126.

[47] E. Lieb, T. Schultz and D. Mattis, *Two soluble models of an antiferromagnetic chain*, Annals of Physics **16**(3), 407 (1961), doi:https://doi.org/10.1016/0003-4916(61)90115-4.

[48] T. Koffel, M. Lewenstein and L. Tagliacozzo, *Entanglement entropy for the long-range ising chain in a transverse field*, Phys. Rev. Lett. **109**, 267203 (2012), doi:10.1103/PhysRevLett.109.267203.

[49] M. Gabbrielli, L. Lepori and L. Pezzè, *Multipartite-entanglement tomography of a quantum simulator*, New Journal of Physics **21**(3), 033039 (2019), doi:10.1088/1367-2630/aafb8c.

[50] S. Fey and K. P. Schmidt, *Critical behavior of quantum magnets with long-range interactions in the thermodynamic limit*, Phys. Rev. B **94**, 075156 (2016), doi:10.1103/PhysRevB.94.075156.

[51] B. Žunkovič, A. Silva and M. Fabrizio, *Dynamical phase transitions and Loschmidt echo in the infinite-range XY model*, Phil. Trans. R. Soc. A. **374** (2016), doi:10.1098/rsta.2015.0160.

[52] A. Das, K. Sengupta, D. Sen and B. K. Chakrabarti, *Infinite-range ising ferromagnet in a time-dependent transverse magnetic field: Quench and ac dynamics near the quantum critical point*, Phys. Rev. B **74**, 144423 (2006), doi:10.1103/PhysRevB.74.144423.

[53] A. Dutta and J. K. Bhattacharjee, *Phase transitions in the quantum ising and rotor models with a long-range interaction*, Phys. Rev. B **64**, 184106 (2001), doi:10.1103/PhysRevB.64.184106.

[54] E. Gonzalez-Lazo, M. Heyl, M. Dalmonte and A. Angelone, *Finite-temperature critical behavior of long-range quantum Ising models*, SciPost Phys. **11**, 76 (2021), doi:10.21468/SciPostPhys.11.4.076.

[55] M. Foss-Feig, Z.-X. Gong, C. W. Clark and A. V. Gorshkov, *Nearly linear light cones in long-range interacting quantum systems*, Phys. Rev. Lett. **114**, 157201 (2015), doi:10.1103/PhysRevLett.114.157201.

[56] A. S. Buyskikh, M. Fagotti, J. Schachenmayer, F. Essler and A. J. Daley, *Entanglement growth and correlation spreading with variable-range interactions in spin and fermionic tunneling models*, Phys. Rev. A **93**, 053620 (2016), doi:10.1103/PhysRevA.93.053620.

[57] B. Žunkovič, M. Heyl, M. Knap and A. Silva, *Dynamical quantum phase transitions in spin chains with long-range interactions: Merging different concepts of nonequilibrium criticality*, Phys. Rev. Lett. **120**, 130601 (2018), doi:10.1103/PhysRevLett.120.130601.

[58] J. C. Halimeh and V. Zauner-Stauber, *Dynamical phase diagram of quantum spin chains with long-range interactions*, Phys. Rev. B **96**, 134427 (2017), doi:10.1103/PhysRevB.96.134427.

[59] R. Khasseh, A. Russomanno, M. Schmitt, M. Heyl and R. Fazio, *Discrete truncated wigner approach to dynamical phase transitions in ising models after a quantum quench*, Phys. Rev. B **102**, 014303 (2020), doi:10.1103/PhysRevB.102.014303.

[60] F. H. L. Essler and M. Fagotti, *Quench dynamics and relaxation in isolated integrable quantum spin chains*, Journal of Statistical Mechanics: Theory and Experiment **2016**(6), 064002 (2016).

[61] L. S. Levitov, H. Lee and G. B. Lesovik, *Electron counting statistics and coherent states of electric current*, Journal of Mathematical Physics **37**(4845) (1996), doi:https://doi.org/10.1063/1.531672.

[62] M. Esposito, U. Harbola and S. Mukamel, *Nonequilibrium fluctuations, fluctuation theorems, and counting statistics in quantum systems*, Rev. Mod. Phys. **81**, 1665 (2009), doi:10.1103/RevModPhys.81.1665.

[63] M. Campisi, P. Hänggi and P. Talkner, *Colloquium: Quantum fluctuation relations: Foundations and applications*, Rev. Mod. Phys. **83**, 771 (2011), doi:10.1103/RevModPhys.83.771.

[64] P. Calabrese, M. Collura, G. D. Giulio and S. Murciano, *Full counting statistics in the gapped xxz spin chain*, Europhysics Letters **129**(6), 60007 (2020), doi:10.1209/0295-5075/129/60007.

[65] M. Collura, F. H. L. Essler and S. Groha, *Full counting statistics in the spin-1/2 heisenberg xxz chain*, Journal of Physics A: Mathematical and Theoretical **50**(41), 414002 (2017), doi:10.1088/1751-8121/aa87dd.

[66] M. Collura and F. H. L. Essler, *How order melts after quantum quenches*, Phys. Rev. B **101**, 041110 (2020), doi:10.1103/PhysRevB.101.041110.

[67] D. J. Luitz, N. Laflorencie and F. Alet, *Many-body localization edge in the random-field heisenberg chain*, Phys. Rev. B **91**, 081103 (2015), doi:10.1103/PhysRevB.91.081103.

[68] R. Singh, J. H. Bardarson and F. Pollmann, *Signatures of the many-body localization transition in the dynamics of entanglement and bipartite fluctuations*, New Journal of Physics **18**(2), 023046 (2016), doi:10.1088/1367-2630/18/2/023046.

[69] M. Gring, M. Kuhnert, T. Langen, T. Kitagawa, B. Rauer, M. Schreitl, I. Mazets, D. A. Smith, E. Demler and J. Schmiedmayer, *Relaxation and prethermalization in an isolated quantum system*, Science **337**(6100), 1318 (2012), doi:10.1126/science.1224953.

[70] Y. Tang, W. Kao, K.-Y. Li, S. Seo, K. Mallayya, M. Rigol, S. Gopalakrishnan and B. L. Lev, *Thermalization near integrability in a dipolar quantum newton's cradle*, Phys. Rev. X **8**, 021030 (2018), doi:10.1103/PhysRevX.8.021030.

[71] B. Blaß and H. Rieger, *Test of quantum thermalization in the two-dimensional transverse-field ising model*, Scientific Reports **6** (2016), doi:10.1038/srep38185.

[72] D. M. Greenberger, M. A. Horne and A. Zeilinger, *Going Beyond Bell's Theorem*, pp. 69–72, Springer Netherlands, Dordrecht, doi:10.1007/978-94-017-0849-4 (1989).

[73] D. Bouwmeester, J.-W. Pan, M. Daniell, H. Weinfurter and A. Zeilinger, *Observation of three-photon greenberger-horne-zeilinger entanglement*, Phys. Rev. Lett. **82**, 1345 (1999), doi:10.1103/PhysRevLett.82.1345.

[74] S. Paeckel, T. Köhler, A. Swoboda, S. R. Manmana, U. Schollwöck and C. Hubig, *Time-evolution methods for matrix-product states*, Annals of Physics **411**, 167998 (2019), doi:10.1016/j.aop.2019.167998.

[75] F. Verstraete, J. J. García-Ripoll and J. I. Cirac, *Matrix product density operators: Simulation of finite-temperature and dissipative systems*, Phys. Rev. Lett. **93**, 207204 (2004), doi:10.1103/PhysRevLett.93.207204.

[76] A. H. Werner, D. Jaschke, P. Silvi, M. Kliesch, T. Calarco, J. Eisert and S. Montangero, *Positive tensor network approach for simulating open quantum many-body systems*, Phys. Rev. Lett. **116**, 237201 (2016), doi:10.1103/PhysRevLett.116.237201.

[77] A. Dutta and J. K. Bhattacharjee, *Phase transitions in the quantum ising and rotor models with a long-range interaction*, Phys. Rev. B **64**, 184106 (2001), doi:10.1103/PhysRevB.64.184106.

[78] E. G. Lazo, M. Heyl, M. Dalmonte and A. Angelone, *Finite-temperature critical behavior of long-range quantum ising models*, SciPost Phys. **11**, 076 (2021), doi:10.21468/SciPostPhys.11.4.076.

[79] S. Birnkammer, A. Bastianello and M. Knap, *Prethermalization in confined spin chains*, doi:10.48550/ARXIV.2202.12908 (2022).

[80] A. H. Werner, D. Jaschke, P. Silvi, M. Kliesch, T. Calarco, J. Eisert and S. Montangero, *Positive tensor network approach for simulating open quantum many-body systems*, Phys. Rev. Lett. **116**, 237201 (2016), doi:10.1103/PhysRevLett.116.237201.

[81] D. Jaschke, S. Montangero and L. D. Carr, *One-dimensional many-body entangled open quantum systems with tensor network methods*, Quantum Science and Technology **4**(1), 013001 (2018), doi:10.1088/2058-9565/aae724.